Study of Energy Transfer Mechanism for a Synchrotron X-ray Gas Absorber with COMSOL Multiphysics.

Álvaro Martín Ortega[1*], Yves Dabin[1], Ana Lacoste[2], Tiberiu Minea[3]
[1]Euroepan Synchrotron Radiation Facility, [2]Laboratoire de Physique Subatomique et Cosmologie, [3]Laboratoire de Physique des Gaz et des Plasmas.
*71, Avenue des Martyrs, 38000 Grenoble, France, alvaro.martin-ortega@esrf.fr

Abstract: The high power delivered by 4th generation X-ray sources makes necessary the use of absorbers to reduce the heat load on the critical optical elements. At the ESRF, a gas absorber will be installed in the upgraded beamline ID31. A complete model of the system requires taking into account ionization in the bulk of the gas, diffusion and recombination of the charged particles, thermalization of the high-energy electrons and heat transfer. In this work we present the results from two models: one to study the effect of thermal convection in the heat transfer, and one to study the diffusion and recombination of the ions and electrons generated. The comparison of the model results with the experimental ones shows some differences coming from the necessary approximations made in the model.

Keywords: Gas attenuator, Synchrotron, Plasma, Recombination.

1. Introduction

X-ray beams delivered by modern synchrotron and free electron lasers can reach power densities up to 300 W/mm^2 and total power of a few kW [1-2]. To protect the optical elements of the beamline, usually a monochromator, absorbers are placed in the beam path to remove the low energy photons while letting pass the high energy ones (figure 1). A gas absorber has the advantage of being a stress free medium which only needs the walls of the vessel to be cooled. However, gas ionization and heating modifies the central density, making difficult to predict the final absorption.

The gas attenuator installed in ID31 consist on a 1-m long cylinder of 12 mm radius, with standard ESRF diamond windows at both ends to isolate the rest of the beamline, under vacuum. The cylinder is connected to a variable belly to vary the volume available to the gas, changing this way the density and absorption. The vessel is cooled by water flowing through a double wall. A noble gas like Argon or Krypton is used to avoid chemical reactions between the ions and the walls.

In order to understand the different energy transfer processes, we have set up two COMSOL models. In the first one, we have studied the effect of the thermal convection over the heat transfer, assuming a 2D geometry and comparing the results with and without gas flow. In the second one, we have studied the distribution of ions and excited species and the fraction of energy spent in heating the gas, assuming a 1D axisymmetric geometry.

2. Heat transfer model

2.1 Numerical model

We want to solve the Navier-Stokes equation for a compressible, stationary, non-isothermal flow subject to the gravity force:

$$\nabla \cdot (\rho u) = 0$$

$$\rho(u \cdot \nabla)u = \nabla \cdot (-pI + \tau) + \rho g$$

$$\rho C_p (u \cdot \nabla)T = -\big(\nabla(k\nabla T)\big) + \tau S - \frac{T}{\rho}\frac{\partial \rho}{\partial T}(u \cdot \nabla)p + Q$$

Where τ is the viscous stress, S the strain-rate tensor and k the thermal conductivity of the gas.

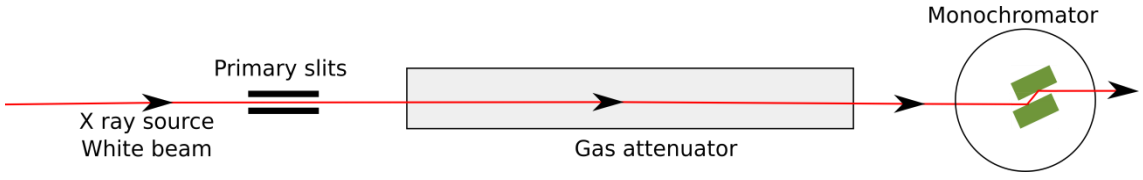

Figure 1: Schematic setup of a gas absorber.

The material properties are taken as those of the Kr, which means that both the thermal conductivity and the viscosity are pressure-independent. No other forces than gravity are applied on the system: the gas flow will be due exclusively to the gravity force.

The geometry of the system is a disc of 12 mm radius, with a vertical symmetry axis. The gas is heated in a central square of 2 mm side, and the walls temperature is fixed at 300 K. By doing a 2D model we are assuming that the gradients in the longitudinal direction are negligible compared to those on the radial direction. A parametric sweep was set up with

pressure range between 50 and 500 mbar and a power input between 1 and 700 W/m.

Two adimensional numbers are used to quantify the effect of the convection in the heat transfer: Rayleigh and Nusselt numbers [3]. The Rayleigh number is the equivalent to the Reynolds number in buoyancy-driven flows: at low values the flow will be laminar, while at high values it will be turbulent. It is, in turn, the product of the Prandtl and Grashoff numbers: the ratio of thermal to viscous diffusion and the ratio of buoyancy to viscous forces. The Nusselt number is the ratio between the local heat transfer at a wall and the average one. Its value is 1 for pure thermal conduction in planar geometries, and will increase as the convection increases. Both numbers are related: a more intense flow (high Ra) will mean a more efficient heat transfer by convection (high Nu).

$$Ra = \frac{C_p \mu}{k} \cdot \frac{g \rho_0 (T_h - T_c) L^3}{T_0 \mu_0^2}$$

$$Nu = \frac{L}{k_0 (T_h - T_c)} \cdot k \left. \frac{\partial T}{\partial x} \right|_{wall}$$

For non-planar geometries the lower limit of the Nusselt number can be lower or higher than one. To normalize it, we run two simulations for each pair of pressure and power parameters, one with and one without the gravity force. The Nusselt number used will be the ratio between both cases.

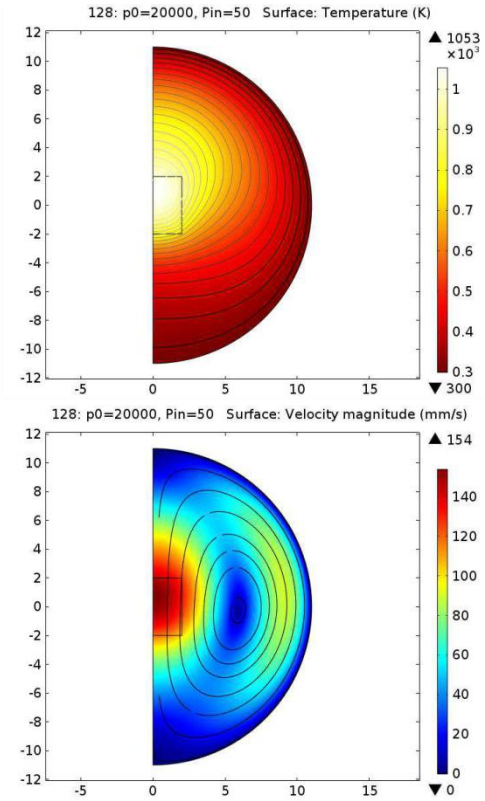

Figure 2: Temperature (top) and velocity (bottom) profiles of the gas for 200 mbar and 50 W input.

3.2 Results and discussion

An example of the temperature and velocity profiles obtained is shown in figure 2. The gas velocity does not exceed 0.16 m/s and the temperature profile is only slightly distorted from the axially symmetric one, as opposed to the plume of hot gas at constant temperature which characterizes convective flows.

The plots of Ra vs Nu numbers are shown in fugure 3, linked by constant pressure and by constant input power. For constant power, the higher values are achieved when the pressure is higher. However, for constant pressure, the higher values are reach at a power around 20-50 W and decrease for even higher power. The reason for this behavior is that the gas velocity has a limit given by the maximum density difference, while the thermal conduction does not:

$$\Delta\rho = \rho_c - \rho_h = \frac{p}{R}\left(\frac{1}{T_c} - \frac{1}{T_h}\right)$$

If $T_h \to \infty$ then $\Delta\rho \to \frac{p}{RT_c}$

In all the cases, the values of the Nusselt and Rayleigh numbers indicate that the flow of the gas is laminar and that the thermal convection has little to no impact on the heat transfer and on

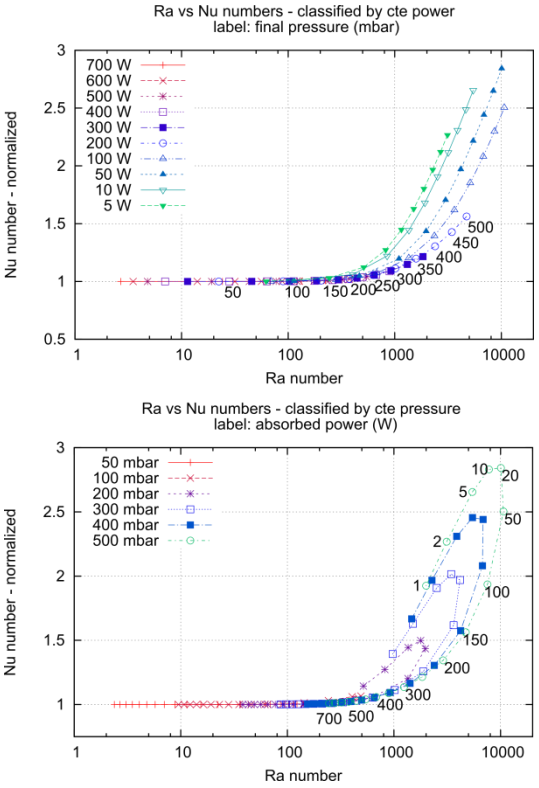

Figure 3: Na vs Ra numbers, linked by constant power (top) and pressure (bottom)

the temperature result. This will simplify further calculations, since it will be enough to consider the heat transfer by conduction to obtain a realistic result.

3. Plasma model

3.1 Numerical model

The objective of the plasma model is to determine what exact fraction of energy is spent on heating the gas. To do this, diffusion of charged particles and electro-chemical reactions have to be taken into account, as well as the radiative deexcitation of the excited species. The plasma and the heat transfer interfaces are used to this end.

Six Krypton species plus the electrons are considered: ground state, first and second (Krs and Krp) excited states, mono- and diatomic ions (Kr+ and Kr2+) and excited dímer (Kr2s). Only 15 reactions (Table 1) are included due to the scarce bibliography compared to other gases as Argon. In any case, the dominant reaction of every kind is already included in the model.

The transport coefficients and the reaction rates 1 to 6 have been calculated using the BOLSIG+ software, assuming a maxwellian EEDF, and then introduced in the model as temperature-dependent coefficients. Reaction 7 was included ad dependent on electron and gas temperature; reactions 8 to 12 were included as constant coefficients due to the lack of information on the temperature-dependence; and reactions 13 to 15 are radiative decays and constant by definition.

	Reaction	References
1	$e + Kr \Rightarrow e + Kr$	[4] LXCat
2	$e + Kr \Rightarrow e + Kr^s$	
3	$e + Kr \Rightarrow e + Kr^p$	
4	$e + Kr^s \Rightarrow e + Kr$	
5	$e + Kr^p \Rightarrow e + Kr$	
6	$e + Kr \Rightarrow 2e + Kr^+$	
7	$e + Kr_2^+ \Rightarrow Kr + Kr^p$	[5]
8	$e + Kr_2^s \Rightarrow Kr^s + Kr + e$	[6]
9	$2Kr + Kr^+ \Rightarrow Kr + Kr_2^+$	
10	$2Kr^s \Rightarrow e + Kr + Kr^+$	
11	$2Kr_2^s \Rightarrow e + 2Kr + Kr^s$	
12	$Kr^s + 2Kr \Rightarrow Kr + Kr_2^s$	
13	$Kr^s \Rightarrow Kr + hv$	[7]
14	$Kr^p \Rightarrow Kr^s + hv$	[8]
15	$Kr_2^s \Rightarrow 2Kr + hv$	[6]

Table 1: list of included reactions.

The geometry of the system is a 1D axisymmetric segment of 12 mm length. The centre of symmetry is the centre of the gas cylinder, and the opposite extreme the wall. The plasma source is defined by a Gaussian function centered in the axis of symmetry and σ=1mm. This represents the scattering of the initial high energy electrons until they are slowed down to a

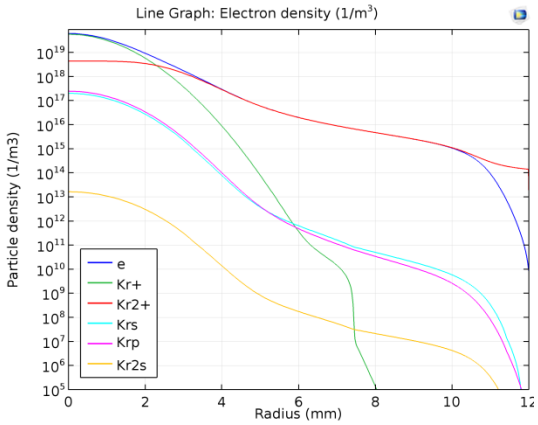

Figure 4: Particle profiles for 200 mbar and a source of 1E20 e/s/m

thermal energy, further ionizing and exciting atoms in the process. The geometrical source is the the same for electrons, monoatomic ions and excited species. The wall of the attenuator is grounded and it's a perfect sink of electrons, ions and excited species. The reemission coefficients are set to 0. The stabilization coefficients are set to 3 to reduce the non-physical reaction of particles.

We run simulations for a range of pressures between 50 and 500 mbar and power inputs between 20 and 1000 W/m. This power was not set directly but through the total electron and ions source: the same number of electrons, ions and excited species (equally distributed among Krs and Krp), and an energy source for the electrons assuming 4 eV for initial electron.

4.2 Results and discussion

The results show that the main ion is the Kr2+ everywhere except for the lowest pressure and higher power input, and only in the centre of the cylinder. Also, virtually all the recombination takes place in the bulk of the plasma, with the density near the sheath orders of magnitude below that on the centre. In the most extreme case, at 50 mbar, only 0.007% of the

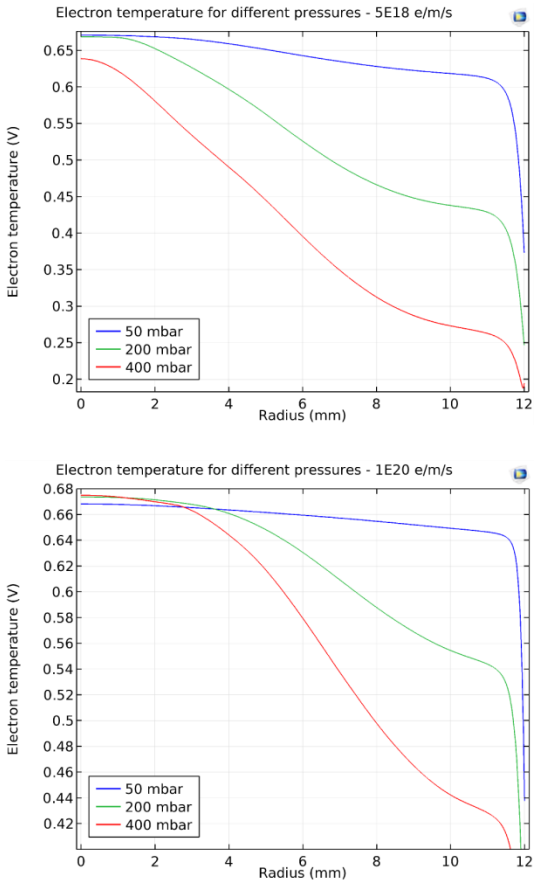

Figure 5: Electron temperature profiles for different cases.

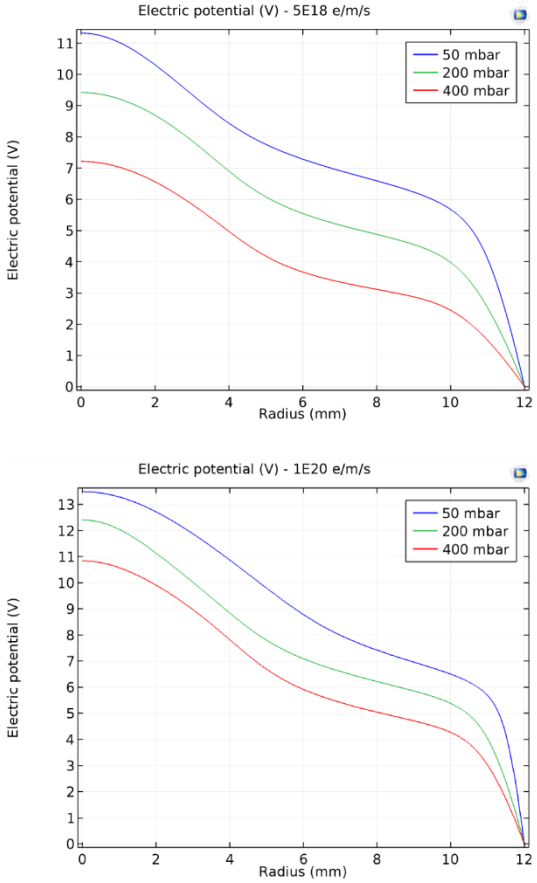

Figure 6: Plasma potential profiles for different cases

recombination occurs in the walls.

A common result on all the cases is an central electron temperature around 0.65 eV, with the decrease near the walls taking different shapes. Also the plasma potential goes from 6-7 V at the centre for low input and increases up to 12 V; increasing further the source will not increase the plasma potential either.

Only a small fraction of the input power heats up the gas. The main sink of the excited species is the radiative deexcitation. This means that most of the power input as excited species will not heat up the gas, as well as the power carried by the excited species after recombination.

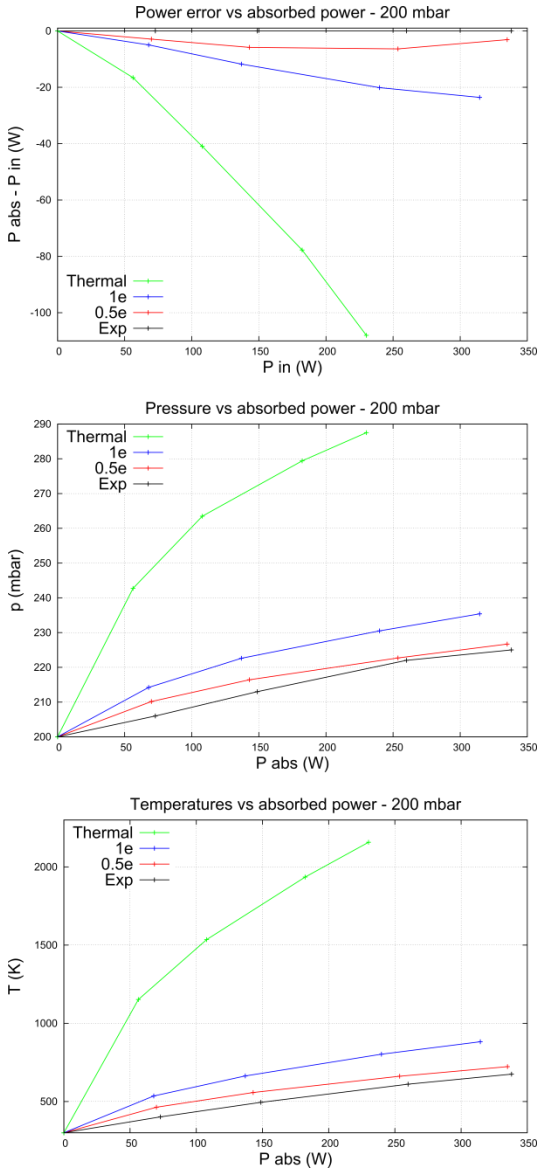

Figure 7: Model vs. experimental results, for the case of 200 mbar.

5. Comparison with experiment

To compare the results from both thermal and plasma models with the experiments [10], a lookup table was created including central density, input power and pressure. Then, a preudo-3D model was set up in which we stack a series of 2D discs with different power input, as the X-ray beam gets absorbed, and a common pressure. This common pressure is the final one; the initial one is calculated from the final solution, using mass conservation and including all the volume of gas connected to the cylinder.

We can see in figure 4 that the thermal results depart from the experimental ones by a large amount, meaning that important physical phenomena is omitted. The plasma model gives a much closer to the experimental ones, but it is still not enough to fit the data. A possible source of error is the plasma source properties. Reducing the electron and ion source to a half and increasing the excited species one by 1.5, meaning an increase of radiative deexcitation and a decrease on recombination and heating, improves the result but it is still not enough to account for the difference.

Other than the plasma source and the balance of particles, there are many points where the model could be improved. The EEDF has been assumed maxwellian but could have a very different shape. This could have an impact on the transport coefficients and reaction rates, modifying the overall power balance. Another source of error is that the slowing down of the electrons has not been considered in detail. In this process, a charge separation could appear that would lead to a different geometrical source for each species.

6. Conclusions

The different energy transfer mechanisms in an X-ray gas attenuator have been studied using different modules of COMSOL. The effect of thermal convection of the gas was modeled using

the CFD and heat transfer modules, and was found to be negligible in comparison to the thermal conduction. The ionization and excitation of the gas atoms was modeled using the Plasma module, giving a more realistic picture of the processes. Most of the power is lost via radiative deexcitation, with virtually all the electron recombining in the bulk of the plasma. The dominant ion is the Kr_2^+, except at low pressure and high ionization densities.

The pseudo 3-D model built from the outputs of the COMSOL models shows that a correct description of the plasma phenomena is essential to build a realistic model of the system. The rough approximations made here give an approximate result, enough to help us to understand the processes inside but not to design future attenuators.

1. L. Zhang et. al. Thermal deformation of cryogenically cooled silicon crystals under intense X-ray beams: measurement and finite-element predictions of the surface shape, *J. Sync. Rad.*, **20**, 567-580 (2013)

2. Jean Susini et. Al. New challenges in beamline instrumentation for the ESRF Upgrade Programme Phase II, *J. Sync. Rad*, **21** 986-995 (2014)

3. W. Rosenhow et. al., Handbook of heat transfer fundamentals, 1985 McGraw-Hill.

4. Biagi-v8.9 database, www.lxcat.net, retrieved on June 1, 2015 / Cross sections extracted from Program Magboltz, Version 8.9 March 2010

5. P. Lukáč et. al., Dependence of the dissociative recombination of molecular ions Kr2+ with electrons on the electron and gas temperatures, *Plasma Sources Sci. Tech.*, **21** 065002 (2012)

6. S. Bendella et. al., Modelling of Kr-Xe discharge of sxcimer lamp, *EPJ Web of Conferences*, **44** 04004 (2013) and references therein.

7. A. Delâge and J-D Carette, Oscillator strengths of Kr I electronic transitions measured by electron spectrometry, *J. Phys. B: Atom. Molec. Phys.*, **14** 2399 (1976)

8. W.E. Ernst and E. Schilz-Gulde, Transition probabilities for Kr I lines from wall-stabilized arc measurements, *Physica* **93C** 136-144 (1978)

9. C. Flores, Study of a gas absorber for Synchrotron's light, Master Thesis, UPM (2010)